Dielectric heating effects on the activity and SO2 resistance of La0.8Ce0.2MnO3 perovskite for methane oxidation

Zhang, Y.; Castricum, H.L.; Beckers, J.; Eiser, E.; Bliek, A.

Published in:
Journal of Catalysis

DOI:
10.1016/j.jcat.2003.09.016

Microwave energy effects on activity and SO_2 resistance of $La_{0.8}Ce_{0.2}MnO_3$ perovskite for methane oxidation

Y. Zhang-Steenwinkel, H.L. Castricum, J. Beckers, E. Eiser, A. Bliek*

Department of Chemical Engineering, University of Amsterdam, Nieuwe Achtergracht 166, 1018 WV Amsterdam, The Netherlands

Corresponding author: A. Bliek,

Tel: 31-20-5256479

Fax: 31-20-5255604

bliek@science.uva.nl

ABSTRACT

The oxidative catalytic activity towards CH_4 of a $La_{0.8}Ce_{0.2}MnO_3$ perovskite is investigated under dielectric and conventional heating conditions. As these materials are both microwave sensitive and catalytically active, they may be applied as coating material for ceramic soot filters for the reduction of soot emission from Diesel engines. Dielectric heating is shown to result in a much higher CH_4 conversion and a higher resistance to SO_2 poisoning. We propose that local hot spots on the catalytic surface explain the increased activity toward CH_4 conversion. The catalytic activity in SO_2 is largely maintained, as pore blockage by sulphates, as experienced in conventional heating, is counteracted.

Keywords: Perovskites, $La_{0.8}Ce_{0.2}MnO_3$, microwave, SO_2 poisoning, methane oxidation.

1. INTRODUCTION

Whereas Diesel engines have favourable engine efficiency and therefore contribute to the reduction of green house gases, environmental pollution by diesel-engine exhausts in the form of soot particulate matter is of increasing concern [1-3]. Due to the carcinogenic nature of soot, soot emission standards will be tightened drastically in Europe in the coming 5 years. For this reason, substantial efforts are devoted to the development of new catalytic after-treatment processes [4]. Several techniques have been developed to deal with soot emissions, such as the use of homogenous fuel additives (passive regeneration) and the use of inert or catalytically active filters. Using catalytic soot filters may reduce energy consumption. Ciambelli et al. [5] showed that a reduction of the soot ignition temperature by about 180 K is possible using a Cu/V/K/Cl/Ti coated ceramic filter. Teraoka et al. [6,7] studied new catalysts for simultaneous NO_x-soot removal, in particular spinel-type (AB_2O_4) and K_2NiF_4-type (A_2BO_4) materials. These authors found that the catalytic performance of the spinels depends to a significant extent on the constituent metal, $CuFe_2O_4$ being superior in terms of selectivity to nitrogen formation, and a low selectivity to nitrous oxide.

Passive regeneration using catalytically active filters is generally not considered feasible for normal low-temperature diesel engine operation. Active regeneration would either require raising the off-gas temperature, for instance, by a modified operation of the engine, or by heating the entire filter element to soot light-off temperatures. From an energetic point of view neither method can be considered to be elegant. An alternative is the use of microwave-assisted regeneration, allowing instantaneous and energetically efficient heating [8,9]. As dielectric heating is a bulk technique, it is faster than heating based on conduction. Moreover, yet unexplained and surprisingly high catalytic reaction rates have been reported [10-16]. The present objective is to assess the feasibility of using a

microwave sensitive catalytic material as a soot filter coating. By periodic exposure to a dielectric field, the coating is allowed to reach soot ignition temperatures, resulting in the self-sustained carbon burn-off.

Among different candidate materials, perovskite-type oxides have been reported as active catalysts in the oxidation of CO, hydrocarbons and chlorinated hydrocarbons, as well as in automotive exhaust catalysis [17-20]. As compared to noble metals, perovskite-based catalysts pair a comparable activity to a high resistance to deactivation by hydrothermal sintering, and low cost [21]. Moreover, these oxides are high loss dielectric materials [22,23], which render them suitable for the present purpose. Perovskites can be described by the general structural formula $ABO_{3\pm\delta}$, with A generally a lanthanide ion and B a transition metal ion. A and B can both be partially substituted by other ions, which leads to a wide variety of mixed oxides, $A_{1-x}A'_xB_{1-y}B_y'O_{3\pm\delta}$. δ is a measure of the number of structural and electronic defects and corresponding cation/anion vacancies due to non-stoichiometry [21]. In earlier work [24], we demonstrated that for La-Mn based perovskites, these vacancies contribute to the catalytic activity in full oxidation.

To assess the practicality of these perovskites for the present purpose, we need to establish their sensitivity to SO_2 poisoning under the conditions relevant to automotive operations [25]. As SO_2 has a high electronic affinity, depending on the reaction temperature and composition of the perovskites, the sulphur species, SO_2, SO_3, SO_3^{2-}, SO_4^{2-} and S^{2-} have all been reported [25,26].

Presently, SO_2 poisoning is investigated for $La_{0.8}Ce_{0.2}MnO_3$ prepared by co-precipitation, and used in CH_4 oxidation as a model reaction, in both conventional and dielectric heating experiments. The composition and surface structure of sulphur-poisoned catalyst have been studied using FTIR, XRD, XPS, TPR and TEM.

2. EXPERIMENTAL

2.1 Catalyst synthesis and characterisation

The perovskite-type oxide $La_{0.8}Ce_{0.2}MnO_3$ was prepared by co-precipitation, according to the method described in elsewhere [18,24]. The chemical composition is assessed using Inductively Coupled Plasma Atomic Emission Spectroscopy (ICP–AES) on a multichannel Thermo Jarrel Ash ICAP 957 spectrometer, upgraded to ICAP 61. The specific surface area and pore volume were measured by nitrogen adsorption at 77 K on a Sorptomatic 1990 (CE Instruments) and evaluated using the BET equation. The density of the perovskite is measured by a Multivolume Pycnometer 1305 using He as filling gas. Crystallographic analysis was carried out by powder X-ray diffraction (XRD) on SR 5069 using a PW 1830 generator with $2\theta = 10 - 90°$, CuKα radiation. Data with respect to chemical composition and physical properties are summarised in table 1.

Infrared spectra were optained on a Bio-Rad FTS 45A system equipped with a MCT detector with a resolution of 2 cm^{-1} in a range of 400 cm^{-1} to 4000 cm^{-1}.

The core levels and valence electronic structure of the catalysts were studied using X-ray photoelectron spectroscopy (XPS) on a VG ESCAlab 210i-XL spectrometer with Mg Kα (1253.6 eV) as the excitation source. The spectra were recorded in the fixed analyser transmission mode with pass energy 70 eV and at pressures less than 10^{-10} mbar. The core level of La 3d, Mn 2p, S 2p and Ce 4d species were recorded and relative intensities $I_{S\ 2p}/I_{(La\ +\ Mn)}$ determined.

TEM images were obtained on a JEOL 2010 Transmission Electron Microscope (point to point resolution of 0.23 nm and lattice image resolution of 0.14 nm) operated at 200 keV with a LaB_6 filament. All images were collected using a Gatan multiscan ccd camera (model 791).

The catalysts were reduced in a thermo-gravimetric analysis (TGA) set-up. About 200 mg of sample, weighted to ± 0.1 mg accuracy, was heated in the flow of a H_2/Ar mixture (v/v 2/1, SV = 1.00 x 10^{-2} $m^{-3}{\cdot}s^{-1}{\cdot}kg^{-1}$, Praxair, 99,999%). During reduction, the temperature was raised at 2.5 $K{\cdot}min^{-1}$ to 1073 K and kept at this temperature for one hour. The composition of the exit gas stream was analysed using mass spectrometry. The same experiments for about 15 mg of sample were also carried out in a temperature programmed reduction set-up (TPR) equipped with a TCD in a flowing H_2/Ar mixture (v/v 2/1, SV = 2 x 10^{-2} $m^{-3}{\cdot}s^{-1}{\cdot}kg^{-1}$, Praxair, 99,999%). For reference, TPR patterns of pure $La_2(SO_4)_3{\cdot}xH_2O$ (Aldrich, 99.9%) were obtained.

2.2 Microwave set-up

The dielectric heating system used is a travelling wave once-through set-up, with microwave radiation being absorbed by a water load after passing through the microwave cavity. The system consists of a microwave source (2.45 GHz, 1 kW), a circulator, a three-stub tuner section, a monomode microwave cavity TE_{10}, and a water load, (figure 1). The reflection of the microwaves is minimised using the stub tuners. The wave-guide is formed by a rectangular copper channel (7.21 cm width x 3.605 cm height). The microwave source is protected from the reflected radiation by using a circulator. The temperature in the sample bed is assessed using an optical fibre (Luxtron). A quartz sample tube (i.d. = 18 mm), designed to accommodate the optical fibre is placed perpendicular to the direction of propagation, allowing the sample bed to be uniformly exposed to microwave radiation. The optical fibre is calibrated using thermocouples. 3.35 g of $La_{0.8}Ce_{0.2}MnO_3$ perovskite (10 cm^3) was placed in the reactor and kept in place by a quartz grid, subsequently heated to 423 K in a He flow (GHSV = $6{\cdot}10^2$ hr^{-1}) with a heating rate of 5 K min^{-1}, followed by stabilisation at 423 K for one hour. The bulk temperature of the sample

was monitored simultaneously with a thermocouple and an optical fibre. The lower detection limit of the optical fibre is 373 K.

2.3 CH_4 oxidation experiments over $La_{0.8}Ce_{0.2}MnO_3$

After the calibration of the optical fiber, methane oxidation over $La_{0.8}Ce_{0.2}MnO_3$ was carried out by both dielectric and conventional heating using a CH_4 (Praxair, 99.995%)/O_2 (Praxair, 99.5%)/He (Praxair, 99.999%) gas mixture (v/v/v 5/12.5/82.5, GHSV = $12 \cdot 10^2$ hr^{-1}) at a temperature of 423 K – 723 K (figure 2).

2.4 SO_2 poisoning experiments of $La_{0.8}Ce_{0.2}MnO_3$

The resistance to SO_2 poisoning was investigated by addition of 200 ppm SO_2 (Praxair, 1007 ppm SO_2 in He) to the gas feed either at 723 K or at room temperature during temperature programmed experiments. In both cases, the catalytic activity was assessed at 723 K. Gas composition analysis was performed using an Interscience gas chromatograph equipped with four capillary columns (2 x Porabond Q, Molsieve plot and Alumina), two flame ionisation detectors (FID) and two thermal conductivity detectors (TCD).

3. RESULTS

3.1 Catalytic activity of $La_{0.8}Ce_{0.2}MnO_3$ in CH_4 oxidation

$La_{0.8}Ce_{0.2}MnO_3$ activity data in CH_4 oxidation are presented in figure 3a, showing the conversion versus temperature for both conventional and dielectric heating. Surprisingly, the CH_4 conversion reached is substantially higher for dielectric heating.

3.2 SO_2 deactivation of $La_{0.8}Ce_{0.2}MnO_3$ in CH_4 oxidation

The influence of the presence of SO_2 on CH_4 oxidation was tested using 200 ppm SO_2 in the feed. Two types of experiments were carried out. In the first, the catalyst was brought to the reaction temperature and subsequently 200 ppm SO_2 was added to the feed stream. When the catalyst was exposed for an extended time-on-stream (15 hours) at 723 K in the absence of SO_2, followed by 15 hours at the same reaction temperature in the presence of SO_2, no significant deactivation was observed for either of the heating modes (not shown).

When SO_2 was added at 298 K, and the catalyst was subsequently subjected to a temperature-programmed experiment, a loss in activity is observed, both in conventional and dielectric heating experiments (figure 3b). After prolonged exposure, an irreversible deactivation is observed for conventional heating to about half of the initial activity. For dielectric heating, the activity drops only slightly to about 95% of its original level at 723 K (figure not shown).

The deactivation observed is accompanied by the formation of white and yellow coloured separate phases. The yellow fraction was mainly observed for dielectric heating, whereas the white fraction was mostly present after conventional heating. The poisoned perovskites were analysed by XRD, FTIR, XPS and TEM. No significant differences between the fresh sample and the poisoned samples are detectable by XRD (figure 4), suggesting that the SO_2-poisoned phase exists either in amorphous form or in particle sizes below the detection limit of XRD (2 nm). FTIR spectra of the catalysts deactivated by SO_2 show bands between 1000 and 1300 cm^{-1} (figure 5). These bands can be assigned to bulk sulphates [27,28].

The surface composition of the fresh, as well as the white and the yellow fractions from the deactivated catalysts were studied by XPS. The resulting binding energy values were corrected using the C 1s peak at 285 eV. In table 2, the corresponding binding energies of La 3d, Mn 2p and S 2p for the fresh sample and the yellow and white fractions from the

poisoned samples are listed. The binding energy of S 2p was about 169.2 eV for both fractions, which can be attributed to sulphate [26,29]. No peak was found at a binding energy of 167.3 eV, corresponding to sulphite, implying that only sulphates were formed [26,29]. The binding energy of La $3d_{5/2}$ in the fresh sample is 834.6 eV, and those of the yellow and white fraction are 836.0 eV and 836.4 eV, respectively (figure 6a). This is an indication for the formation of $La_2(SO_4)_3$ species, which has a binding energy of 836.5 eV [26, 29]. The binding energy of Mn $2p_{5/2}$ in the yellow and white fraction, at 641.4 eV and 641.6 eV respectively, is lower than the one in the fresh sample (642.2 eV), and similar to the binding energy of MnO. This suggests formation of a separate MnO phase from the mixed oxide. The binding energy at 122.0 eV and 125.7 eV (figure 6b) refers to the Ce $4d_{5/2}$ and Ce $4d_{3/2}$ components, respectively, with the spin-orbit splitting of 3.5 eV [30]. These peaks are characteristic for Ce^{4+} with a Ce $4d^9$ - O $2p^6$ - Ce $4f^0$ final state [30], thus indicating a cerium oxide phase. In the white fraction, however, the intensity seems to be much lower than in the fresh sample or the yellow fraction.

TEM images taken after the reaction (figure 7) show that sintering has occurred for the white and yellow fraction of the catalyst after CH_4 oxidation (b and c). The white fraction shows massive sintering as compared to the fresh catalyst (a). In contrast, in the yellow fraction, predominantly formed in the dielectrically heated sample, small particles are left on the edge of the big cluster. N_2 adsorption measurements confirm that strong sintering has occurred during conventional heating. Using BET surface area data and pore volume data the mean pore diameter after SO_2 poisoning during dielectric heating is assessed to be about 6.5 nm, and for conventional heating it is about 3.5 nm. Sintering may reduce the number of catalytically active sites and limit the accessibility of the active sites towards the reactants.

The phases formed during deactivation were more closely investigated by TPR (figure 8). TPR data of the SO_2 poisoned catalyst during conventional heating show a similar profile

as pure $La_2(SO_4)_3 \cdot xH_2O$. Reduction takes place in two steps with peaks at 862 K and 966 K. In contrast, the catalyst deactivated in a dielectric field shows a broad reduction band. After a H_2 treatment in the TGA, XRD patterns have been recorded for the fresh sample and the poisoned ones both in the dielectric and conventional oven (figure 9). The samples have become grey/green after reduction at 1073 K, suggesting the formation of new phases. The XRD pattern reveals the disappearance of the perovskite phase, with concurrent formation of individual La_2O_3, MnO and Ce_2O_3 for the fresh sample. The XRD data obtained from both deactivated catalysts shows a strong characteristic peak of lanthanide oxide sulphide (La_2O_2S), formed by reduction of lanthanum sulphate. No evidence was found for the formation of $MnSO_4$ in the presence of SO_2. A small amount of Ce_2S_3 was observed after the reduction treatment for the poisoned sample only when conventional heating was used.

4. DISCUSSION

4.1 Catalytic performance in conventional and dielectric heating

The catalytic activity in CH_4 full oxidation is considerably higher during dielectric heating than during conventional heating. It has been postulated that dielectric heating may result in selective heating of catalytic sites with respect to their direct surroundings, thus leading to “molecular hot spots” [31]. When a material contains strongly absorbing active sites such as dipoles, microwave energy will be absorbed selectively by active sites and these so-called “hot spots” will be generated. The A- and B-sites of perovskite-type oxides have been shown to have different dipole strengths [32]. Therefore, “hot spot” formation is possible for perovskites during dielectric heating. Reactant molecules adsorbed on such a “hot active site” may be activated by subsequent energy transfer from the site to the adsorbed molecule. The difference between local temperature of the “hot spots” and the bulk mean temperature can be up to several hundreds of degrees [ref]. Generation of hot

spots is of great importance in heterogeneous catalysis because reactions on active sites may take place at much higher temperatures than at the measured bulk temperature of the catalyst. Therefore, the reaction rate can be much higher than under conventional heating.

For supported metal catalysts, this effect is also strongly metal particle size dependent. Based on the measurements on size-dependent conductivity using microwave frequencies, Nimtz et al. [33] suggested that the conductivity decreases from the bulk value approximately as the cube of the diameter for particles smaller than 500 nm, leading to the highest/lowest temperatures for very small particles (??). A more conventional explanation for the higher rate may simply be that due to the bulk heating nature of dielectric heating, the intraparticle temperature may be substantially higher than the surface temperature during dielectric heating, for similar surface temperatures.

4.2 Deactivation by SO_2

A loss in catalytic activity in the kinetic regime is observed for both heating modes. This may be due to the competitive adsorption between gas phase oxygen and SO_2, since methane oxidation at low temperature is a suprafacial reaction involving oxygen coming from gas phase or sitting at the oxygen vacancies of the catalysts [34]. The superior catalytic performance for dielectric heating in the presence of SO_2 introduced in the gas feed at 298 K is in line with the results from Turner et al. [35]. They observed an improved performance for a commercial Pt-Rh based three-way automotive catalyst (Engelhard) poisoned by SO_2 for combined dielectric/conventional heating, as compared to conventional heating only. This result was attributed to selective absorption of microwave radiation by sulphides and sulphates, with subsequent decomposition towards SO_2.

Our results indicate that neither for dielectric heating nor conventional heating a significant loss in catalytic activity occurs when SO_2 is added at 723 K. Alifanti et al. [36] observed that $La_{0.9}Ce_{0.1}CoO_3$, $La_{0.8}Ce_{0.2}CoO_3$ and $La_{0.8}Ce_{0.2}MnO_3$ compositions are least sensitive to SO_2 poisoning from the series of $La_{1-x}Ce_xMn_{1-y}Co_yO_3$ perovskites (x = 0, 0.1, 0.2, 0.3 and y = 0.5, 0.6, 0.7) at 823 K. Following a 15 hour period exposure at 823 K to 20 ppm SO_2 added to the feed, the activity in methane oxidation was shown to remain at a stable level in excess of 80 % of the original value. Our deactivation data – indicating that deactivation is limited when SO_2 is added at high temperature – strongly suggest that this is the result of weak adsorption of SO_2 at these temperatures, which may additionally arise from the competitive adsorption of H_2O produced in the oxidation reaction (figure not shown).

After prolonged exposure of the catalysts to SO_2 at 298 K, and the subsequent temperature programmed reaction, formation of bulk sulphates was observed by FTIR measurements. The surface electronic(?) structure recorded by XPS of the white and yellow fractions obtained after SO_2 poisoning shows that $La_{0.8}Ce_{0.2}MnO_3$ is deactivated predominantly by irreversible formation of lanthanum sulphate. This is confirmed by the XRD patterns of the reduced poisoned samples, which indicate a strong characteristic peak of Lanthanide oxide sulphide formed during the reduction of the sulphate. Formation of MnO is observed by XPS and XRD, while no evidence is found for the formation of Mn sulphates. Finally, XPS data show a decrease in the Ce 4d peak intensity for the white fraction, indicating that the original Ce oxidic structure has been destroyed, most likely due to the formation of Cerium sulphate. This is also confirmed by XRD data after reduction: a characteristic peak of Ce_2S_3 is observed for the reduced poisoned sample when conventional heating is used.

Since the poisoned sample using dielectric heating mainly contains the yellow fraction, poisoning in the microwave mainly affects the La cation by formation of $La_2(SO_4)_3$. For

conventional heating, SO_2 poisoning affects both La and Ce cations by formation of sulphates, as indicated by the predominant presence of the white fraction. The $I_{S/I_{(La + Mn)}}$ ratio, as determined by XPS (table 2), shows that the white fraction contains 50 % more sulphate species than the yellow fraction. The formation of cerium sulphates can be considered indicative of the destruction of the anion vacancies, which are responsible for the catalytic activity.

4.3 SO_2 poisoning mechanism over $La_{0.8}Ce_{0.2}MnO_3$ during the heating

During both dielectric and conventional heating, the presence of SO_2 leads to an irreversible formation of lanthanum sulphate and thus to deactivation of the catalyst. It is known that the concentration of sulphates increases with rising reaction temperature, as the formation of sulphates is controlled by the reaction kinetics (29). During conventional heating (based on thermal conduction), the exterior of the particles is highest in temperature and the formation rate of formed lanthanum sulphates is thus highest in this region. Therefore, deactivation predominantly takes place at the exterior of the particles through a shell progressive mechanism (figure 10a). The formation of sulphates is accompanied by pore blockage, as indicated by TEM and BET data. This deactivation process thus results in limitation of the access to the catalytic surface. In contrast, the interior of the catalytic particle is highest in the temperature during dielectric heating, based on its bulk heating nature , by creating an effectively *inverse* temperature gradient throughout the catalytic particle. For this reason, deactivation by formation of sulphates occurs predominantly in the interior of the catalytic particles as a result of the high temperature in the interior of the particles. Thus, deactivation during dielectric heating proceeds through a growing core mechanism, as shown in figure 10b. Moreover, the temperature gradient persists for both heating modes, even in steady state, due to the exothermic nature of the reaction. Whereas the activity is thus lost by lanthanum sulphate

formation, the impact of pore blockage is only limited. The exterior of particles is still accessible to reactants and deactivation is slower than during conventional heating. This seems to be confirmed by TPR data: the broad reduction peak found over a temperature range of 200 K for dielectrically heated sample is likely to be the result of (slow) diffusion of H_2 into the centre of the catalyst particle, which subsequently reduces the formed sulphate.

5. CONCLUSION

The high catalytic activity towards CH_4 oxidation over $La_{0.8}Ce_{0.2}MnO_3$ perovskite observed during dielectric heating, as compared with that during conventional heating, can be explained by the higher particle centre temperature, which in turn is the result of the bulk heating nature of dielectric heating. Deactivation of the perovskite by SO_2 is comparatively slow at high temperatures, as a result of weak adsorption of SO_2. Irreversible loss in activity occurs after prolonged exposure of the catalyst to SO_2 due to the formation of Lanthanum sulphate. Cerium sulphate is formed predominantly during conventional heating, which contributes to deactivation by elimination of anion vacancies that are responsible for the catalytic activity. Deactivation is faster for conventional heating than for dielectric heating. This is to be attributed to the concerted effort of lanthanum sulphate formation and the resulting pore blockage, which limits the accessibility towards the reactants. When these phenomena arise predominantly at the external surface via a shell progressive mechanism, as is the case during conventional heating, the result is a fast deactivation. In contrast, when sulphate formation mainly occurs in the particle interior (through a growing core mechanism), as is the case during dielectric heating, pore blockage plays no major role and deactivation is less dramatic.

ACKNOWLEDGEMENT

The financial support of Netherlands Research Council for this project is gratefully acknowledged. Thanks are due to Mr. R. Haswell and Mr. G. Jonkers from Shell Research & Technology Centre for the performing TEM and XPS, to Mr. T. Visser, F. Soulimani from the University of Utrecht and Mr. L.M. van der Zande from the University of Amsterdam for FT-IR, to Mr. J. Elgersma for ICP, and Mrs. M.C. Mittelmeijer-Hazeleger for N_2 adsorption measurements.

REFERENCES

[1] S. Ponce, M.A. Peña, J.L.G. Fierro, Appl. Catal. 27 (1996) 107.

[2] S.S. Hong, G.D. Lee, Catal. Today 63 (2000) 397.

[3] Y. Teraoka, K. Kanada, S. Kagawa, Appl. Catal. 34 (2001) 73.

[4] P. Zelenka, W. Cartellieri, P. Herzog, Appl. Catal. 10 (1996) 3.

[5] P. Ciambelli, V. Palma, P. Russo, S. Vaccaro, Ind. Eng. Chem. Res. 39 (2000) 4914.

[6] W.F. Shangguan, Y. Teraoka, S. Kagawa, Appl. Catal. 8 (1996) 217.

[7] Y. Teraoka, K. Nakano, W. Shangguan, S. Kagawa, Catal. Today 27 (1996) 107.

[8] J.X. Ma, M. Fang, P. Li, B. Zhu, X.H. Lu, N.T. Lau, Appl. Catal. 159 (1997) 211.

[9] J.W. Tang, T. Zhang, L. Ma, N. Li, D.B. Liang, L.W. Lin, J. Catal. 211 (2002) 560.

[10] P. Lidström, J. Tierney, B. Wathey, J. Westman, Tetrahedron 57 (2001) 9225.

[11] J.W. Tang, T. Zhang, D.B. Liang, H.H. Yang, N. Li, L.W. Lin, Appl. Catal. 36 (2002) 1.

[12] N. Kuhnert, Angew. Chem. Int. Ed. 41 (2002) 1863.

[13] A. Stadler, S. Pichler, G. Horeis, C.O. Kappe, Tetrahedron 58 (2002) 3177.

[14] R. Pérez, T. Beryozkina, O.I. Zbruyev, W. Haas, C.O. Kappe, J. Comb. Chem. 4 (2002) 501.

[15] G.A. Strohmeier, C.O. Kappe, J. Comb. Chem. 4 (2002) 154.

[16] E. Van der Eycken, P. Appukkuttan, W. De Borggraeve, W. Dehaen, D. Dallinger, C.O. Kappe, J. Org. Chem. 67 (2002) 7904.

[17] K.S. Song, H.X. Cui, S.D. Kim, S.K. Kang, Catal. Today 47 (1999) 155.

[18] D. Kieβling, R. Schneider, P. Kraak, M. Haftendorn, G. Wendt, Appl. Catal. 19 (1998) 143.

[19] H.M. Zhang, Y. Shimzu, Y. Teraoka, N. Miura, N. Yamazoe, J. Catal. 121 (1990) 432.

[20] R.J.H. Voorhoeve, D.W. Johnson Jr., J.P. Remeika, P.K. Gallagher, Science 195 (1977) 827.

[21] L. Forni, I. Rossetti, Appl. Catal. 38 (2002) 29.

[22] T.A. Vanderah, C.K. Lowe-Ma, D.R. Gagnon, J. Am. Ceram. Soc. 77 (1994) 3125.

[23] B. Vaidhyanathan, D.K. Agrawal, T.R. Shrout, Y. Fang, Mater. lett. 42 (2000) 207.

[24] Y. Zhang-Steenwinkel, J. Beckers, A. Bliek, Appl. Catal. 235 (2002) 79.

[25] L. Wan, in: L.G. Tejuca, J.L.G. Fierro (Eds.), Properties and Applications of Perovskite-type Oxides, Marcel Dekker, New York, 1993, p. 145.

[26] Y.F. Zhu, R.Q. Tan, J. Feng, S.S. Ji, L.L. Cao, Appl. Catal. 209 (2001) 71.

[27] S. Hodjati, C. Petit, V. Pitchon, A. Kiennemann, Appl. Catal. 30 (2001) 247.

[28] I. Rosso, E. Garrone, F. Geobaldo, B. Onida, G. Saracco, V. Specchia, Appl. Catal. 30 (2001) 61.

[29] H. Wang, Y.F. Zhau, R.Q. Tan, W.Q. Yao, Catal. Lett. 82 (2002) 199.

[30] D.R. Mullins, S.H. Overbury, D.R. Huntely, Surface Sci. 409 (1998) 307.

[31] L. Seyfried, F. Gairn, G. Maire, J.M. Thiébaut, G. Roussy, J. Catal. 148 (1994) 281.

[32] N. Setter, E. Colla, I. Reaney, R. Zurmuehlen, D. Dube, J. Petzelt, Ferroelectrics, 154 (1994) 231.

[33] G. Nimtz, P. Marquardt, J. Crystal Growth 86 (1988) 66.

[34] M.A. Peňa, J.L.G. Fierro, Chem. Rev. 101 (2001) 1981.

[35] M.D. Turner, R.L. Laurence, K.S. Yngvesson, W.C. Conner, Catal. Lett. 71 (2001) 133.

[36] M. Alifanti, A. Auer, J. Kirchnerova, F. Thyrion, P. Grange, B. Delmon, Appl. Catal. 41 (2003) 71.

TABLES

Table 1: the chemical composition and physical parameters of the $La_{0.8}Ce_{0.2}MnO_3$ perovskite

Parameter	Value / crystal phases	Analysis method
Elemental composition (mol mol^{-1} Mn)	La: Ce: Mn = 0.72 : 0.18 : 1	ICP-AES
S_{BET}	43.3 m^2 g^{-1}	N_2 adsorption
Pore volume	0.11 cm^3 g^{-1}	N_2 adsorption
Mean pore diameter	10.1 nm	N_2 adsorption
Density	2.64 g cm^{-3}	Pycnometer
Solid composition	Perovskite/CeO_2	XRD

Table 2: La 3d, Mn 2p and S 2p binding energies for the fresh perovskite, yellow and white fraction, after SO_2-poisoning in the dielectric and conventional oven.

Sample	La 3d (eV)	Mn 2p (eV)	Ce 4d (eV)	S 2p (eV)	$I_S/I_{(La + Mn)}$
Fresh	834.6	642.2	121.5	-	-
	838.5	645.1	125.1		
Yellow fraction	836.0	641.4	122.0	169.2	1.5
	839.2	644.9	125.5		
White fraction	836.4	641.6	122.3	169.5	2.3
	839.6	644.7	125.7		

CAPTIONS TO FIGURES:

Figure 1: Schematic drawing of 2.45 GHz microwave heating system consisting of: microwave source (Muegge, MW); generator (Muegge, MW-GIR 2M); circulator (Philips); stub tuners (Muegge); power sensor (Rhode & Schwarz); optical fiber (Luxtron, Accufiber-OFT straight end lightpipe); microwave chokes and water load. Dashed lines denote heated tubing.

Figure 2: Inlet manifold for the catalysed CH_4 combustion experiment. The quadrupole mass spectrometer (MS) and gas chromatograph are both computer controlled. The gas flow is controlled by mass flow controllers (MFC). Dashed lines denote heated tubing.

Figure 3: CH_4 conversion versus catalyst bed temperature for dielectric and conventional experiments in the presence (a), and absence (b) of 200 ppm SO_2, GHSV = $12 \cdot 10^2$ hr^{-1}.

Figure 4: XRD patterns of the fresh sample and SO_2 (200 ppm) poisoned samples during dielectric and conventional heating: perovskite (o); CeO_2 (Δ).

Figure 5: FT-IR spectra of fresh sample and SO_2 (200 ppm) poisoned samples during dielectric and conventional heating.

Figure 6: XPS La 3d (a) and Ce 4d (b) spectra for the fresh catalyst, and the yellow and white fractions obtained after SO_2-poisoning. Hier moet de grootheid op de y-as nog vermeld worden!!

Figure 7: TEM image of fresh $La_{0.8}Ce_{0.2}MnO_3$ sample (a), the yellow fraction (b) the white fraction (c).

Figure 8: TPR patterns of fresh and spent SO_2-poisoned samples after dielectric and conventional heating, as well as of pure lanthanum sulphate. The temperature was raised with 5 $K \cdot min^{-1}$ to 1073 K and maintained at 1073 K for 1 h.

Figure 9: XRD patterns after H_2 reduction of the fresh catalyst, SO_2 poisoned during dielectric and conventional heating: La_2O_3 (▼); MnO (■); Ce_2O_3 (▲); La_2O_2S (♦); Ce_2S_3 (●).

Figure 10: SO_2 poisoning mechanism over $La_{0.8}Ce_{0.2}MnO_3$ perovskite during conventional heating (a) and dielectric heating (b).

Figure 1

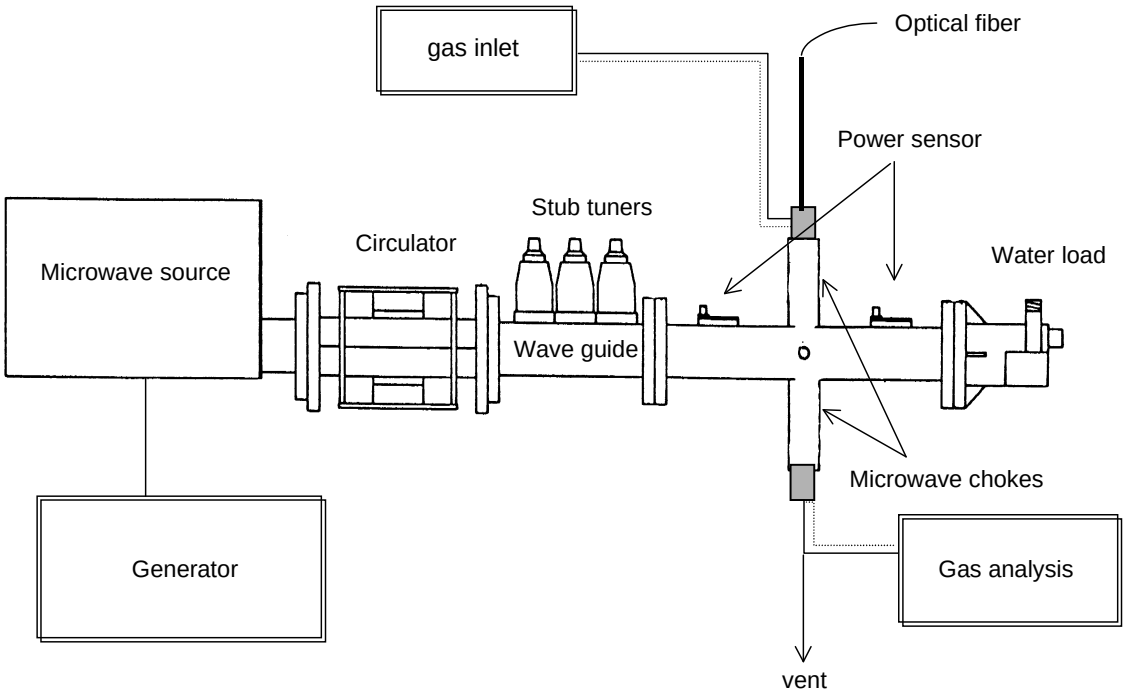
gas inlet
Optical fiber
Power sensor
Stub tuners
Circulator
Microwave source
Water load
Wave guide
Microwave chokes
Generator
Gas analysis
vent

Figure 2

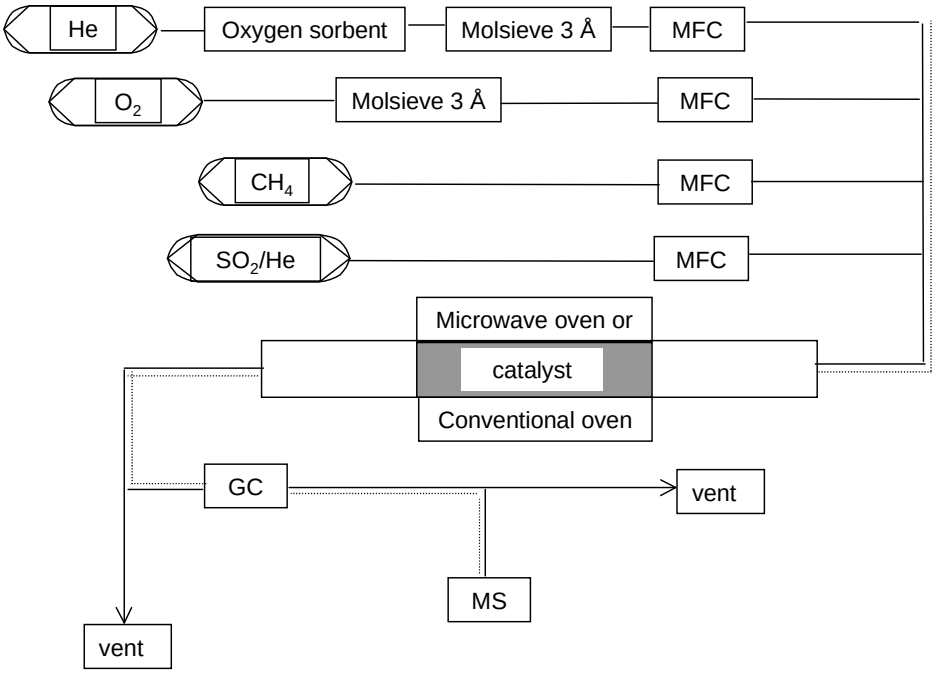
He
Oxygen sorbent
Molsieve 3 Å
MFC
O_2
Molsieve 3 Å
MFC
CH_4
MFC
SO_2/He
MFC
Microwave oven or
catalyst
Conventional oven
GC
vent
MS
vent

Figure 3

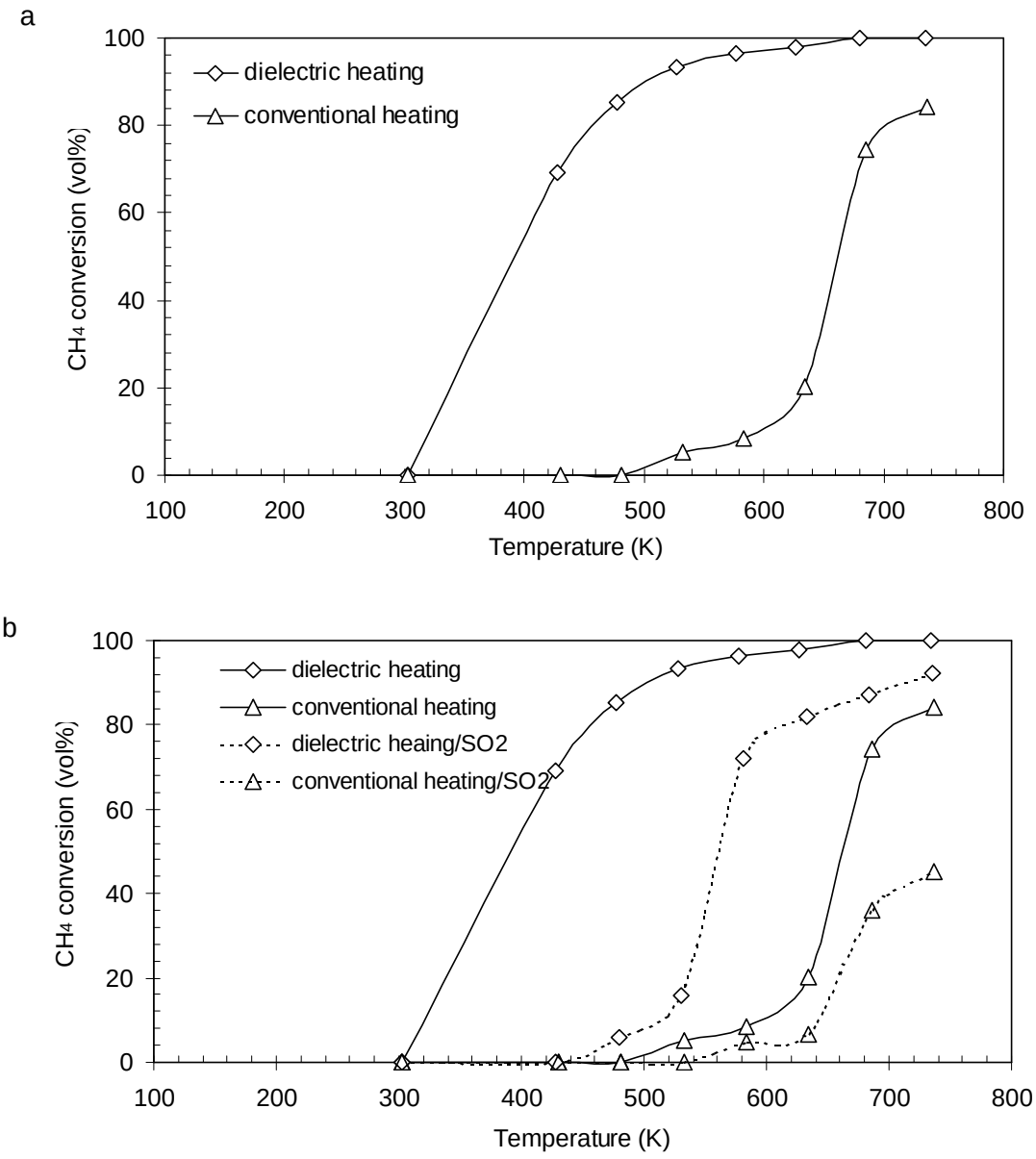
a
100
80
60
40
20
0
CH4 conversion (vol%)
dielectric heating
conventional heating
100
200
300
400
500
600
700
800
Temperature (K)
b
100
80
60
40
20
0
CH4 conversion (vol%)
dielectric heating
conventional heating
dielectric heaing/SO2
conventional heating/SO2
100
200
300
400
500
600
700
800
Temperature (K)

Figure 4

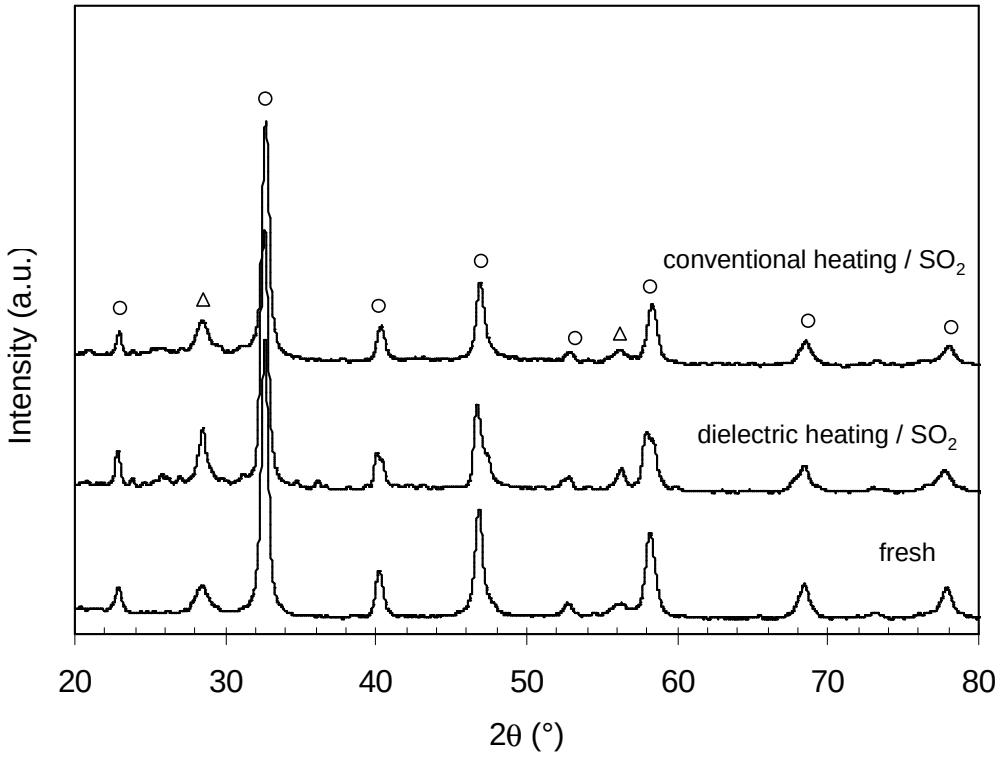
Intensity (a.u.)
conventional heating / SO2
dielectric heating / SO2
fresh
20
30
40
50
60
70
80
2θ (°)

Figure 5

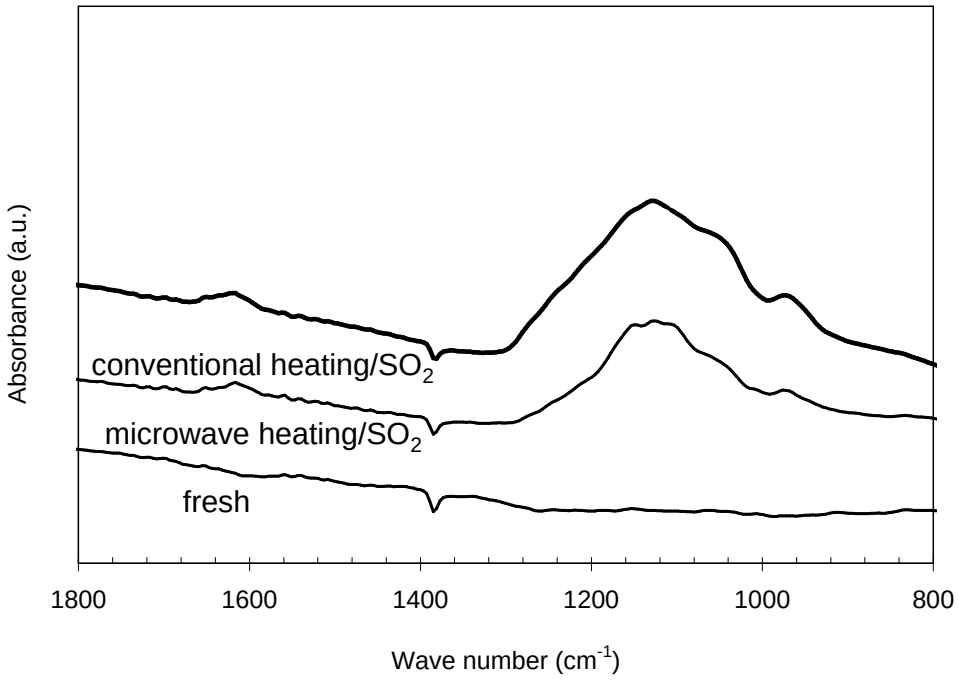
Absorbance (a.u.)
conventional heating/SO2
microwave heating/SO2
fresh
1800
1600
1400
1200
1000
800
Wave number (cm-1)

Figure 6

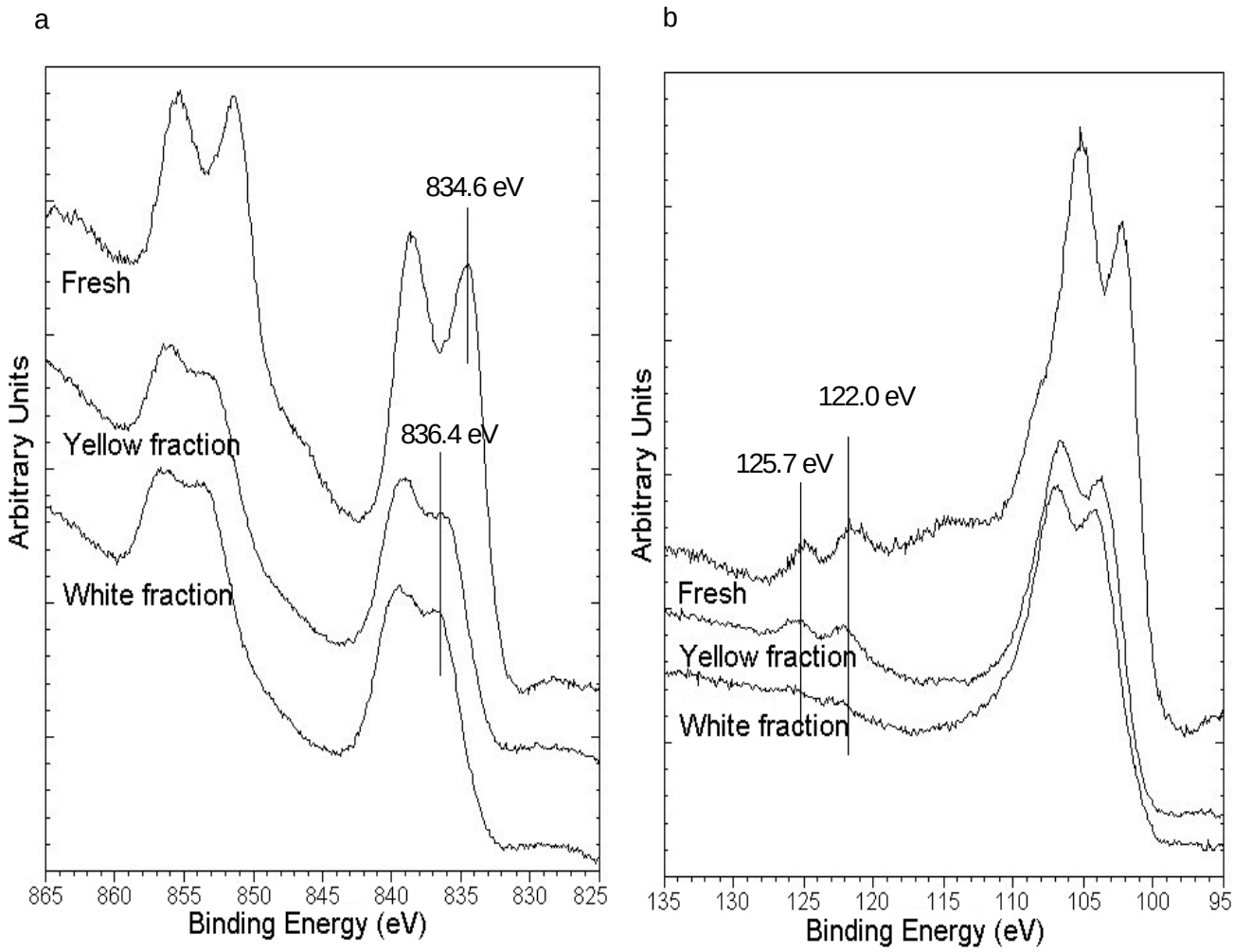
a
b
834.6 eV
836.4 eV
Fresh
Yellow fraction
White fraction
Arbitrary Units
865 860 855 850 845 840 835 830 825
Binding Energy (eV)
122.0 eV
125.7 eV
Fresh
Yellow fraction
White fraction
Arbitrary Units
135 130 125 120 115 110 105 100 95
Binding Energy (eV)

Figure 7

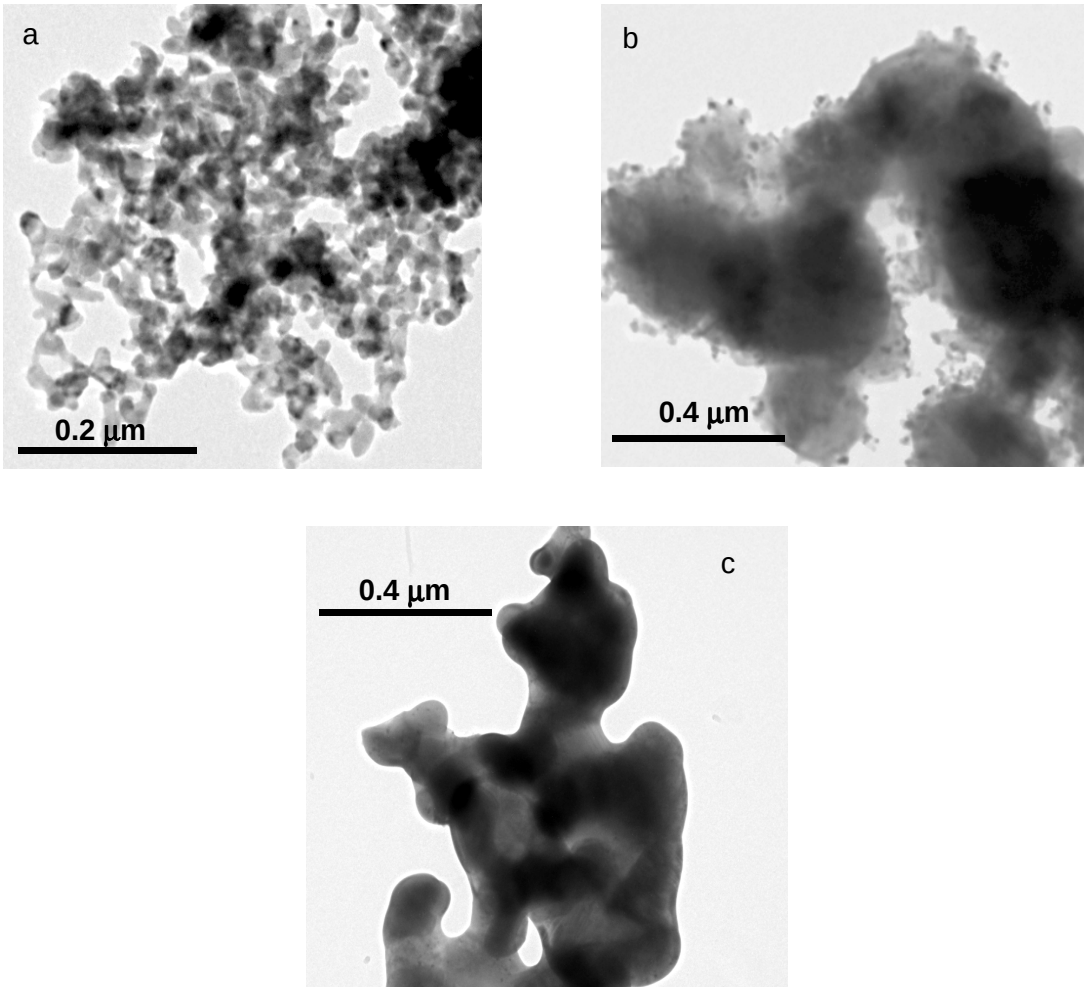

Figure 8

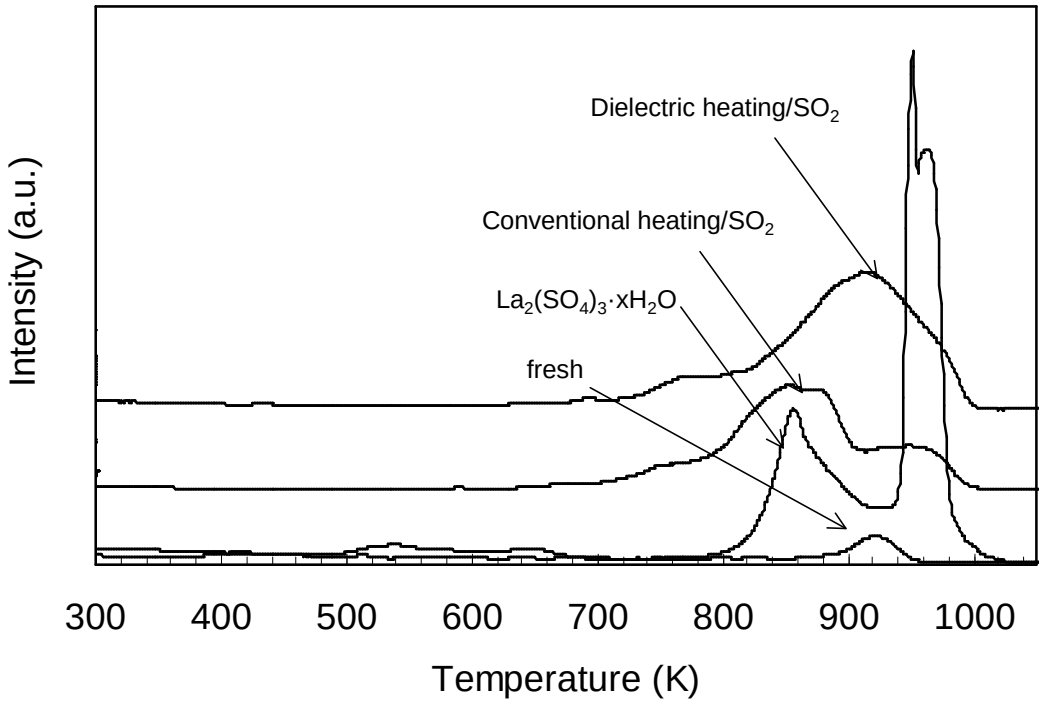
Dielectric heating/SO2
Conventional heating/SO2
La2(SO4)3·xH2O
fresh
Intensity (a.u.)
300
400
500
600
700
800
900
1000
Temperature (K)

Figure 9

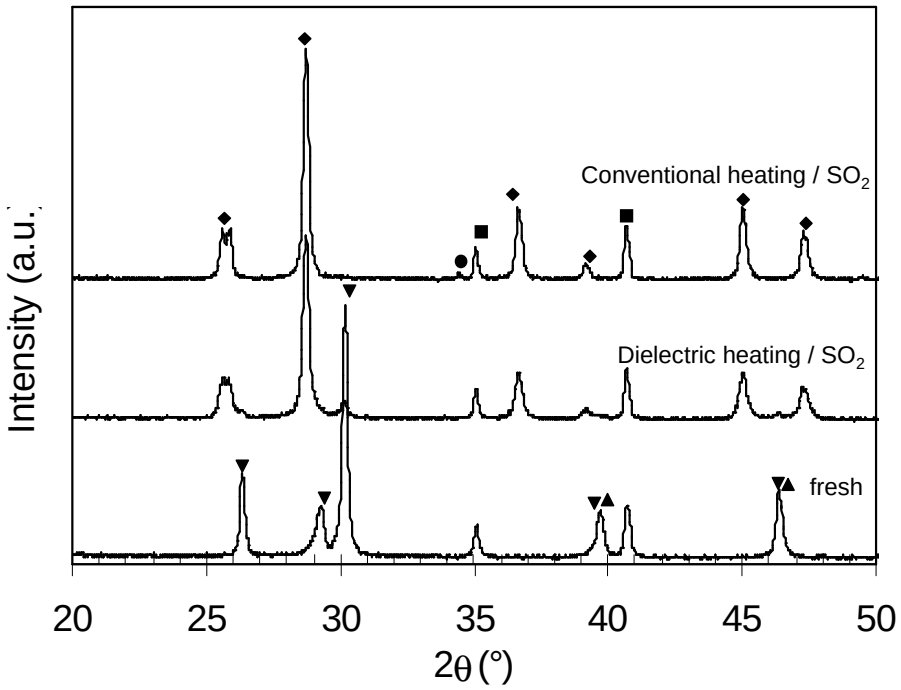
Conventional heating / SO2
Dielectric heating / SO2
fresh
Intensity (a.u.)
20
25
30
35
40
45
50
2θ (°)

Figure 10

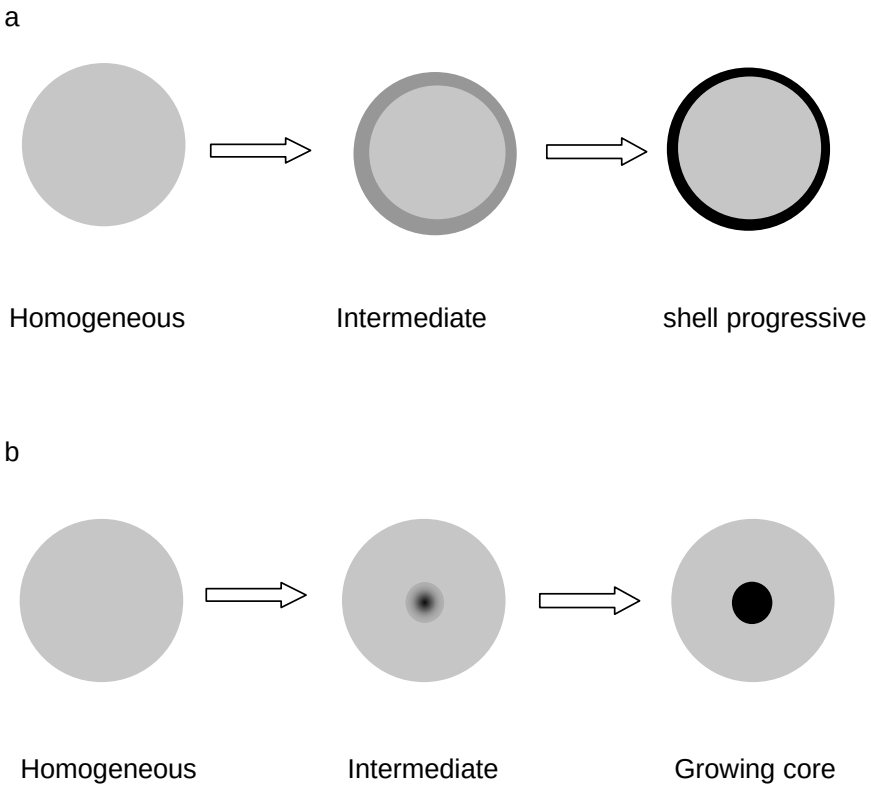
a
Homogeneous
Intermediate
shell progressive
b
Homogeneous
Intermediate
Growing core